Sideband Harmonic Suppression Analysis Based on Vector Diagrams for CHB Inverters under Unbalanced Operation

Jiao, Ning; Wang, Shunliang; Ma, Junpeng; Liu, Tianqi; Zhou, Dao

Published in:
I E E E Transactions on Industrial Electronics

DOI (link to publication from Publisher):
10.1109/TIE.2023.3247797

Publication date:
2024

Document Version
Accepted author manuscript, peer reviewed version

Sideband Harmonic Suppression Based on Vector Diagrams Analysis for CHB Inverters under Unbalanced Operation

Ning Jiao, *Student Member*, *IEEE*, Shunliang Wang, *Member*, *IEEE*, Junpeng Ma, *Member, IEEE*, Tianqi Liu, *Senior Member, IEEE*, Dao Zhou, *Senior Member, IEEE*

***Abstract*- Sideband harmonics of the cascaded H-bridge (CHB) inverters, modulated by the phase-shifted pulse-width modulation (PS-PWM) scheme, will appear with unbalanced dc voltages or/and modulation signals in different cells. The linear controller to suppress the output voltage distortion is destined to be ineffective due to the non-linear characteristic of sideband harmonics. Focus on this problem, this article proposes a closed-loop harmonic suppression method by adjusting the displacement angles for the *N*-cells CHB inverter, with the help of vector diagrams and the Hessian Matrix. This method can achieve the suppression of the harmonic distortion around any multiplicative switching frequency. Displacement angles are adjusted continuously in real-time. No complicated trigonometric function calculations and optimization algorithms are required. The harmonics suppression mechanism is also revealed from a vector synthesis point of view. The superior harmonic performance achieved by the proposed method is verified by the simulation and experiment results.**

***Index Terms*—harmonic suppression, harmonic vectors, cascaded H-bridge inverter, phase-shifted PWM.**

I. Introduction

AMONG varieties of multilevel converters, the cascaded H-bridge (CHB) topology, proposed by McMurray in 1971 [1], is one of the most mature and attractive topologies with high flexibility, and scalability [2]. It achieves excellent output voltage quality due to a large number of power modules and the phase-shifted pulse-width modulation (PS-PWM) technique [3]-[4]. The high-quality output voltage can only be achieved under ideal conditions with equal dc voltages and modulation signals among different cells [5]. Yet, unbalanced conditions are far more common in practice owing to differences in power management or component parameters in each cell. Especially, the imbalance will also be reflected in different modulation signals, even if the dc voltages are controlled to be balanced [6]-[7]. The non-negligible harmonic distortion around the multiplicative switching frequency, dispersed under unbalanced conditions and difficult to be suppressed, may be result in harmonic pollution and even harmonic resonance [8].

Modified methods to mitigate the sideband harmonics under unbalanced conditions are mainly divided into two groups: 1) one specific frequency sideband harmonic elimination based on the fundamental period window; 2) the whole harmonic group elimination based on the carrier signal period window. Variable-angle PS-PWM (VA. PS-PWM) is an attractive way to cancel sideband harmonic at one specific frequency [5], [9]-[13]. Extending the VA. PS-PWM technique to the carrier signal period window, named sampling-time based VA. PS-PWM technique, the elimination of the whole harmonic group is achieved [14]. For the harmonic suppression method in [14], its limitation that the analytical solution of displacement angles exists only when a closed triangle can be formed by the harmonic magnitudes, is explored in [15]. The employment of an extra battery-fed power cell to overcome the limitation is proposed in [16]. Moreover, [17] defines the behavior for the CHB converter operations in the invalid region. To improve the method aforementioned, a discontinuous pulsewidth modulation (D-PWM) is presented to simultaneously work with the VA. PS-PWM technique [18]. However, the methods in [14]-[18] all focus on the most basic topology with the fewest modules, the 3-cells CHB converter. The extension of the method to large number of cells is still limited by complex inverse trigonometric functions. Although extension of the VA. PS-PWM method to be applied to CHB converters with a larger number of cells is briefly introduced in [15], it is not implemented.

For the application of the sampling-time based VA. PS-PWM technique limited by the large number of cells, some methods are also investigated to address the issues by several literature. The problem is initially solved in [19] by forming groups with two or three cells and assigning different roles to different cells. In [20], considering that different combinations result in different performances, an optimization algorithm based on a background task, which contains all possible combinations of cells, is adopted to select the best one. The improved method in [20] achieves the best harmonic performance. The sideband harmonics around both $2f_c$ and $4f_c$ (f_c represents the frequency of the carrier signal) are suppressed for a large extend. The sampling-time based VA. PS-PWM is also successfully applied to the discontinuous-PWM method for *N*-cells CHB converters [21]. The proper displacement angles in [21] are also obtained by forming groups and mathematical search algorithm. Although a superior harmonic performance for CHB converters with a large number of cells is obtained in [20], only complex mathematical algorithms are presented, resulting in unclear harmonic suppression mechanism.

To address this issue, the phasor diagrams are used to calculate the generalized phase shifted angles in [22], achieving a very clear and no complex mathematical optimization algorithm. However, the application range of the method is very limited, since the harmonic vectors should satisfy a closed polygon [22]. Otherwise, the method will lose the ability to eliminate harmonics. And the method in [22] is only suitable

for harmonics around $2f_c$. For sideband harmonics around other multiplicative switching frequency, which may lead to harmonic resonance and should be minimized, the method in [22] will be invalid. Although no worries about this problem nevertheless exist in the method proposed in [20], the background task is used to obtain the proper angles. But it can not cover all the actual complex operational conditions.

Combining with the vector diagrams, this article proposes a closed-loop harmonic suppression method to deal with the harmonic distortion produced by the unbalanced operation of a N-cells CHB converter. With the insightful derivation process, the harmonic suppression mechanism is more clear and comprehensive. The sideband harmonic around any multiplicative switching frequency can be suppressed to its possible minimum, even for conditions when the harmonic vectors do not satisfy a closed polygon. The proposed method achieves continuous adjustment of the displacement angles. The proposed method is applicable for the whole harmonic group elimination based on the carrier signal period window.

The rest of this article is organized as follows. In Section II, the system configuration and harmonic characteristics are introduced. In Section III, the harmonic suppression principle and implement method are elaborated. In Section IV, simulation and experimental tests validate the performance of the proposed method. Section V concludes this article.

II. Harmonic Analysis

The topology of the single-phase CHB inverter and its vector diagram of output voltages are introduced in Fig. 1. The phase-shifted pulse-width modulation (PS-PWM) technique is adopted. i and N denote the cell number and the total number of cells. u_{abi}, U_{dci}, and u_{ab} are the output voltage, dc voltage of cell i, and the sum of all individual cell outputs. u_L, u_s, and i_s are the inductance voltage, the grid-side voltage, and current, respectively. θ_i is the phase angle of u_{abi}.

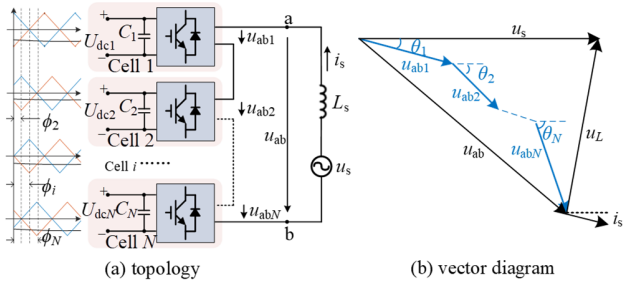

Fig. 1 Topology, and vector diagram of the single-phase CHB inverter.

The output voltage u_{abi} in cell i generated by the unipolar double frequency PWM can be expressed by the classical double Fourier series method [23]:

$$u_{abi}=M_i U_{dci}\cos(\omega_0 t+\theta_i)+\sum_{m=1}^{\infty}\sum_{n=-\infty}^{+\infty} h_{mn}^i \tag{1}$$

$$h_{mn}^i=H_{mn}^i\cos\{[2m\omega_c+(2n+1)\omega_0]t+2m\phi_i+(2n+1)\theta_i\} \tag{2}$$

$$H_{mn}^i=\frac{2U_{dci}}{m\pi}J_{2n+1}(m\pi M_i)\cos[(m+n)\pi] \tag{3}$$

in which M_i, ω_0, and θ_i represent the modulation index, angular frequency, and initial phase angle of the modulation signal in cell i; h_{mn}^i and H_{mn}^i is the sideband harmonic at $[2m\omega_c+(2n+1)\omega_0]$ and its magnitude; m and n are indices to account for carrier and baseband. J_{2n+1} is the Bessel function of $(2n+1)$ order; ω_c is the angular frequency of the carrier signal.

Defining h_m^i as the sum of sideband harmonics h_{mn}^i around the center frequency $2m\omega_c$:

$$h_m^i=\sum_{n=-\infty}^{\infty}h_{mn}^i=\sum_{n=0}^{\infty}(h_{mn}^i+h_{m(-n-1)}^i) \tag{4}$$

Based on the characteristic of the Bessel Function in (5), the sideband harmonic magnitudes H_{mn}^i in (3) satisfy the relationship shown in (6):

$$J_{-n}(\xi)=(-1)^n J_n(\xi) \tag{5}$$

$$H_{mn}^i=H_{m(-n-1)}^i \tag{6}$$

Combining with (2) ~ (4), (6), and the characteristics of trigonometric functions, the sideband harmonics summation in (4) for cell i can be regarded as the harmonic at $2m\omega_c$:

$$h_m^i=a_m^i\cos(2m\omega_c t+2m\phi_i)=\left|a_m^i\right|\cos(2m\omega_c t+\gamma_m^i) \tag{7}$$

in which, a_m^i is the disturbance variable expressed as (8), according to the Jacobi-Anger expansion. $|a_m^i|$ is the harmonic envelope. γ_m^i is the phase angle of the harmonic h_m^i:

$$\begin{aligned}a_m^i&=\sum_{n=0}^{\infty}2H_{mn}^i\cos[(2n+1)\omega_0 t+(2n+1)\theta_i]\\&=\frac{(-1)^m 2U_{dci}}{m\pi}\sin[m\pi M_i\cos(\omega_0 t+\theta_i)]\end{aligned} \tag{8}$$

$$\gamma_m^i=2m\phi_i+g(a_m^i) \tag{9}$$

$$g(a_m^i)=\begin{cases}0, & a_m^i\ge 0;\\ \pi, & a_m^i<0\end{cases} \tag{10}$$

Furthermore, Fig. 2 describes the sideband harmonic summation h_m^i, disturbance variable a_m^i, and the harmonic envelope $|a_m^i|$.

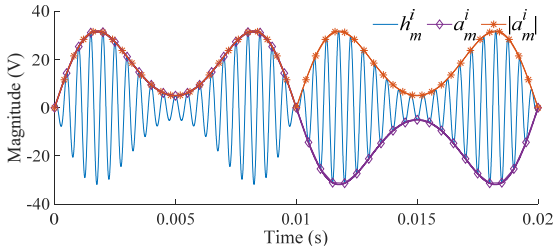

Fig. 2 Relationship of the sideband harmonic summation h_m^i, disturbance variable a_m^i, and the harmonic envelope $|a_m^i|$.

Since all cells are connected in series, the sideband harmonics summation around $2m\omega_c$ in the total output voltage and its envelope can be expressed as

$$h_m=\sum_{i=1}^{N}h_m^i=\sum_{i=1}^{N}\left|a_m^i\right|\cos(2m\omega_c t+\gamma_m^i) \tag{11}$$

$$H_m=\sqrt{[\sum_{i=1}^{N}\left|a_m^i\right|\cos(\gamma_m^i)]^2+[\sum_{i=1}^{N}\left|a_m^i\right|\sin(\gamma_m^i)]^2} \tag{12}$$

Evidently, according to (8), the disturbance variables a_m^i in all cells are identical at any moment, only when the CHB inverter operates under ideal conditions. As shown in Fig. 3 before 0.02s, the harmonic h_m in (11) can be canceled completely. It is benefiting from the uniform distribution of the harmonic vectors in the space as elaborated in Fig. 4 (a), with the displacement angle ϕ_i defined as

$$\phi_i = \frac{i-1}{N}\pi \tag{13}$$

But the harmonic h_m can not be ignored, as shown in Fig. 3 and Fig. 4 (b), due to different disturbance variables a_1^i caused by errors of dc voltages or modulation signals among cells.

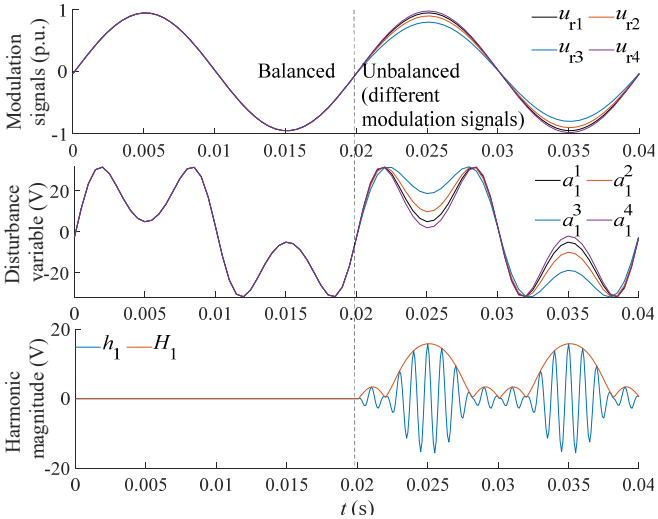

Fig. 3 The modulation signals, the sum of harmonics and its envelope.

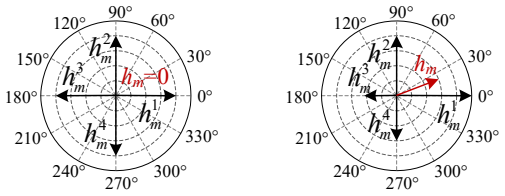

(a) balanced condition (b) unbalanced condition

Fig. 4 Vector diagram of harmonics for 4-cells CHB inverter at time t_c.

III. Harmonic Suppression

A. Harmonic Suppression Principle

For the N-cells CHB inverter, taking the harmonic h_m^i in cell i as the reference, the sum of other individual cell outputs, except for cell i, is defined as

$$h_m^{ex,i} = H_m^{ex,i}\cos(2m\omega_c t + \gamma_m^{ex,i}) = \sum_{k=1,k\neq i}^{N} h_m^k \tag{14}$$

$$H_m^{ex,i} = \sqrt{\sum_{k=1,k\neq i}^{N}(a_m^k)^2 + 2\sum_{x,y\in k}\left|a_m^x\right|\left|a_m^y\right|\cos[2m(\phi_x-\phi_y)+g(a_m^x)-g(a_m^x)]} \tag{15}$$

where, $H_m^{ex,i}$ and $\gamma_m^{ex,i}$ are the envelope and phase angle of $h_m^{ex,i}$, respectively; k represents the k-th cell, except for the i-th H-bridge, (k=1, 2, …, N, $k\neq i$).

The harmonic envelope H_m of the sideband harmonics summation around $2m\omega_c$ in the total output voltage u_{ab} can be rewritten as

$$H_m = \sqrt{\sum_{i=1}^{N}(a_m^i)^2 + 2\sum_{x,y=1,x\neq y}^{N}\left|a_m^x\right|\left|a_m^y\right|\cos[2m(\phi_x-\phi_y)+g(a_m^x)-g(a_m^x)]} \tag{16}$$

Combining with (15) and (16), the harmonic envelope H_m can also be expressed as

$$\begin{aligned} H_m &= \sqrt{\sum_{i=1}^{N}(a_m^i)^2 + \sum_{i=1}^{N}\left|a_m^i\right|H_m^{ex,i}\cos(\gamma_m^i-\gamma_m^{ex,i})} \\ &= \sqrt{\sum_{i=1}^{N}(a_m^i)^2 + \sum_{i=1}^{N}\left|a_m^i\right|H_m^{ex,i}\cos(\langle h_m^i, h_m^{ex,i}\rangle)} \end{aligned} \tag{17}$$

in which, $\langle h_m^i, h_m^{ex,i}\rangle$ represents the included angle between the harmonics h_m^i and $h_m^{ex,i}$, $\langle h_m^i, h_m^{ex,i}\rangle\in[0,\pi]$. The included angle $\langle h_m^1, h_m^{ex,1}\rangle$ is shown in Fig. 5 at time t_c, considering a 4-cells CHB inverter.

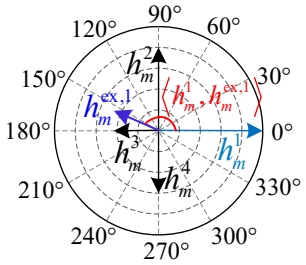

Fig. 5 The included angle $\langle h_m^1, h_m^{ex,1}\rangle$ at time t_c.

From (17) and Fig. 5, the harmonic envelope H_m depends on the included angle $\langle h_m^i, h_m^{ex,i}\rangle$, which is related to the displacement angle ϕ_i. The possibility to suppress the sideband harmonics is provided by applying proper displacement angles. It should be highlighted that the phase angle $\gamma_m^{ex,i}$ of $h_m^{ex,i}$ can be regarded as a constant reference at the instant of operation. From Fig. 5, the value of the included angle $\langle h_m^i, h_m^{ex,i}\rangle$ tends to π, the smaller the harmonic envelop H_m is.

To analyze the influence of displacement angles ϕ_i (i=1, 2, …, N) on the harmonic envelope H_m in (17) mathematically, the Hessian Matrix in (19) is deduced. The Hessian Matrix in (19) is evidently negative semi-definite and positive definite at $\langle h_m^i, h_m^{ex,i}\rangle\in[0,\pi/2]$, and $(\pi/2,\pi]$ (i=1, 2, …, N), respectively. Correspondingly, the harmonic envelope H_m in (17) is a convex function and concave function. And the maximum and minimum values exist respectively at $\langle h_m^i, h_m^{ex,i}\rangle=0$ and $\langle h_m^i, h_m^{ex,i}\rangle=\pi$. Hence, the harmonics can be controlled to the smallest providing that the displacement angles in all the cells satisfy:

$$\left\langle h_m^i, h_m^{ex,i}\right\rangle \to \pi, \quad i=1,2,...,N \tag{18}$$

Considering a 3-cells CHB inverter, the harmonic envelope variation H_1 at different simulation instants (t_1~t_7), with phase differences varying is shown in Fig. 6. The harmonic will

$$A=\begin{bmatrix} \frac{\partial^2 H_m}{(\partial\phi_1)^2} & \frac{\partial^2 H_m}{\partial\phi_1\partial\phi_2} & \cdots & \frac{\partial^2 H_m}{\partial\phi_1\partial\phi_N} \\ \frac{\partial^2 H_m}{\partial\phi_2\partial\phi_1} & \frac{\partial^2 H_m}{(\partial\phi_2)^2} & \cdots & \frac{\partial^2 H_m}{\partial\phi_2\partial\phi_N} \\ \cdots & \cdots & \cdots & \cdots \\ \frac{\partial^2 H_m}{\partial\phi_N\partial\phi_1} & \frac{\partial^2 H_m}{\partial\phi_N\partial\phi_2} & \cdots & \frac{\partial^2 H_m}{(\partial\phi_N)^2} \end{bmatrix}=\begin{bmatrix} \frac{-4m^2 y_1}{\sqrt{z_1}}-\frac{4m^2(x_1)^2}{(z_1)^{3/2}} & 0 & \cdots & 0 \\ 0 & \frac{-4m^2 y_2}{\sqrt{z_2}}-\frac{4m^2(x_2)^2}{(z_2)^{3/2}} & \cdots & 0 \\ \cdots & \cdots & \cdots & \cdots \\ 0 & 0 & \cdots & \frac{-4m^2 y_N}{\sqrt{z_N}}-\frac{4m^2(x_N)^2}{(z_N)^{3/2}} \end{bmatrix} \tag{19}$$

note: $x_i=\left|a_m^i\right|H_m^{\mathrm{ex},i}\sin(\langle h_m^i,h_m^{\mathrm{ex},i}\rangle)$; $y_i=\left|a_m^i\right|H_m^{\mathrm{ex},i}\cos(\langle h_m^i,h_m^{\mathrm{ex},i}\rangle)$; $z_i=\sum_{i=1}^{N}(a_m^i)^2+\sum_{i=1}^{N}\left|a_m^i\right|H_m^{\mathrm{ex},i}\cos(\langle h_m^i,h_m^{\mathrm{ex},i}\rangle)$

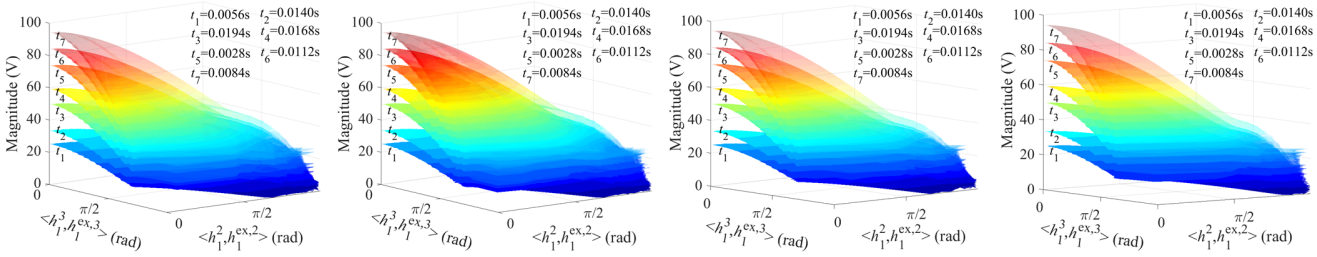

(a) $\phi_1=\pi/18$. (b) $\phi_1=\pi/9$. (c) $\phi_1=\pi/6$. (d) $\phi_1=2\pi/9$.

Fig. 6 The harmonic envelope H_1 for different values of phase angle differences.

decrease with the phase angle differences approaching π, even if the displacement angle ϕ_1 in cell 1 is different. Therefore, the sideband harmonics summation h_m around $2m\omega_c$ can be suppressed with the displacement angles satisfing (18).

In addition, the fact that only the sum of harmonics h_m around $2m\omega_c$ is minimized should be important to highlight. Not all the sideband harmonics h_{mn} at $[2m\omega_c+(2n+1)\omega_0]$ around $2m\omega_c$ achieve the control of the minimum magnitude.

For some situations that only one specific harmonic h_{mn} should be eliminated, its harmonic suppression principle is similar to that of the sideband harmonics summation. The suppression of the harmonic at $[2m\omega_c+(2n+1)\omega_0]$ can achieve with the displacement angles in all the cells satisfying:

$$\left\langle h_{mn}^i,h_{mn}^{\mathrm{ex},i}\right\rangle\to\pi,\quad i=1,2,...,N \tag{20}$$

where, $H_{mn}^{\mathrm{ex},i}$ and $\gamma_{mn}^{\mathrm{ex},i}$ represent the magnitude and phase angle of $h_{mn}^{\mathrm{ex},i}$, which is defined as the sum of individual cell output voltage harmonic at $[2m\omega_c+(2n+1)\omega_0]$, except for cell i.

B. Implementation of the harmonic suppression scheme.

The sideband harmonics suppressing method in the stationary frame is proposed in this subsection.

The function $f(\phi_i)$ is defined as

$$f(\phi_i)=\left|a_m^i\right|H_m^{\mathrm{ex},i}\cos(\gamma_m^i-\gamma_m^{\mathrm{ex},i})+\left|a_m^i\right|H_m^{\mathrm{ex},i} \tag{21}$$

To suppress the harmonic h_m, displacement angle ϕ_i in each cell should satisfy (22), by substituting (18) into (21):

$$f(\phi_i)=\left|a_m^i\right|H_m^{\mathrm{ex},i}\cos(\gamma_m^i-\gamma_m^{\mathrm{ex},i})+\left|a_m^i\right|H_m^{\mathrm{ex},i}\to 0 \tag{22}$$

Combining (9) and (21), the derivative of the function $f(\phi_i)$ with respect to ϕ_i can be expressed as

$$\frac{\mathrm{d}f(\phi_i)}{\mathrm{d}t}=-2m\left|a_m^i\right|H_m^{\mathrm{ex},i}\sin(\gamma_m^i-\gamma_m^{\mathrm{ex},i}) \tag{23}$$

As shown in (23), there is a positive correlation between $f(\phi_i)$ and ϕ_i, and a negative one, when $(\gamma_m^i-\gamma_m^{\mathrm{ex},i})\in(-\pi,0]$ and $[0,\pi]$, respectively.

Hence, the new displacement angle ϕ'_i in each cell can be obtained:

$$\begin{aligned}\phi_i'&=\phi_i-K_C g(\phi_i)f(\phi_i)\\&=\phi_i-K_C g(\phi_i)[\left|a_m^i\right|H_m^{\mathrm{ex},i}\cos(\gamma_m^i-\gamma_m^{\mathrm{ex},i})+\left|a_m^i\right|H_m^{\mathrm{ex},i}]\end{aligned} \tag{24}$$

in which, ϕ_i is the initial displacement angle expressed in (13); K_C denotes the parameters of the controller; $g(\phi_i)$ is the function related to ϕ_i:

$$g(\phi_i)=\begin{cases}1 & \frac{\mathrm{d}f(\phi_i)}{\mathrm{d}t}>0\\ -1 & \frac{\mathrm{d}f(\phi_i)}{\mathrm{d}t}\le 0\end{cases} \tag{25}$$

Based on the displacement angle adjustment method in (24), Fig. 7 describes the angle adjustment of each cell to suppress the harmonic h_1 around $2\omega_c$ for a 4-cell CHB inverter. It can be evidently noticed that the displacement angle ϕ_i should increase, when the phase difference $(\gamma_1^i-\gamma_1^{\mathrm{ex},i})>0$, $(\mathrm{d}f(\phi_i)/\mathrm{d}t<0)$. Otherwise, ϕ_i should decrease. The included angle $\langle h_{mn}^i, h_{mn}^{\mathrm{ex},i}\rangle$ can be controlled to approach π.

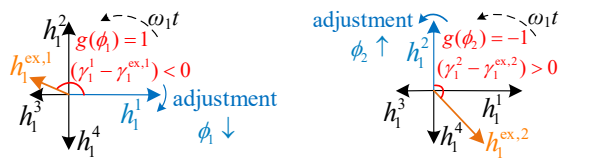

(a) adjustment of cell 1 (b) adjustment of cell 2

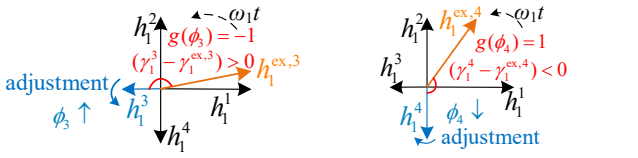

(c) adjustment of cell 3 (d) adjustment of cell 4

Fig. 7 Adjustment of each cell for a 4-cells CHB inverter.

Moreover, even more noteworthy, for some conditions when the harmonic vectors can not form a closed polygon, as shown in Fig. 8, the proposed method is also effective. The harmonic h_m in Fig. 8 reaches the minimum when the largest harmonic vector is opposite to others. So h_m can be suppressed by adjusting the phase difference to satisfy (24).

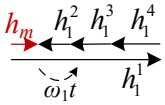

Fig. 8 Harmonic vectors achieve no closed polygons.

For another unfavorable condition when $(\gamma_m^i - \gamma_m^{ex,i})=0$ and $m=N/2$ (cells number N is even), the harmonics vectors h_m^i in each cell are the same or opposite direction in space. The flexibility of the angles adjustment results in the difficulty to obtain the proper angles directly by constructing a closed polygon. Fig. 9 shows the vector diagram of harmonic h_2^i around $4\omega_c$ (m=2) for a 4-cell CHB inverter. Evidently, controlling the included angle to approach π can also achieve based on the displacement angle adjustment method in (24).

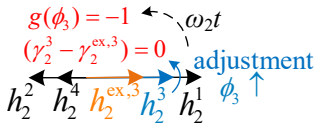

Fig. 9 Adjustment of cell 3 to suppress harmonic h_2 around $4\omega_c$.

The harmonic component h_m^i in (7) can be written as (26) in the stationary:

$$h_m^i = h_m^{i\alpha} + jh_m^{i\beta} \tag{26}$$

$$h_m^{i\alpha} = a_m^i \cos(2m\omega_c t + 2m\phi_i) = \left|a_m^i\right| \cos(2m\omega_c t + \gamma_m^i) \tag{27}$$

$$h_m^{i\beta} = a_m^i \sin(2m\omega_c t + 2m\phi_i) = \left|a_m^i\right| \sin(2m\omega_c t + \gamma_m^i) \tag{28}$$

Hence, the harmonic h_m in the output voltage of the CHB inverter can be expressed as

$$h_m = h_m^{\alpha} + jh_m^{\beta} = (h_m^{i\alpha} + h_m^{ex,i\alpha}) + j(h_m^{i\beta} + h_m^{ex,i\beta}) \tag{29}$$

Combining with (14), (26), (29) and the characteristics of trigonometric functions, the function $f(\phi_i)$ in (22) and (23) can also be written as

$$f(\phi_i) = h_m^{i\alpha} h_m^{ex,i\alpha} + h_m^{i\beta} h_m^{ex,i\beta} + \sqrt{[(h_m^{i\alpha})^2 + (h_m^{i\beta})^2][(h_m^{ex,i\alpha})^2 + (h_m^{ex,i\beta})^2]} \tag{30}$$

$$\frac{df(\phi_i)}{dt} = -2m[h_m^{i\beta} h_m^{ex,i\alpha} - h_m^{i\alpha} h_m^{ex,i\beta}] \tag{31}$$

According to (25), (30), and (31), the flow chart and control diagram of the proposed closed-loop harmonic suppression method is described in Fig. 10: 1) Obtaining the output voltages of the CHB inverter and the i-th H-bridge: u_{ab}, u_{abi}, (or U_{dci}, u_{ri}, ϕ_i). 2) The sum of sideband harmonics h_m and h_m^i selected for suppression are extracted by the band-pass filter or calculated based on (7), (8), and (11). 3) As the pivotal step, the second-order generalized integrator (SOGI) is adopted to obtain the harmonic component in αβ frame, h_m^{α}, h_m^{β}, $h_m^{ex,i\alpha}$, $h_m^{ex,i\beta}$. 4) It is also important to notice that, the displacement angle compensation $\Delta\phi_i$ is obtained by the proportional integral (PI) and proportional resonant (PR) controller based on (30), since $[g(\phi_i) f(\phi_i)]$ contains dc components and even harmonics. And then the new displacement angles ϕ'_i are obtained in real-time by adding the angle compensation $\Delta\phi_i$ into the initial angle ϕ_i.

IV. Experimental Results

To verify the feasibility of the proposed harmonic suppression method, a scaled-down experimental platform for a 4-cells inverter, shown in Fig. 11, is built. The digital signal processor TMS320F28335 is used as the microcontroller. The sideband harmonics summation around $2m\omega_c$, and one dominant specific harmonic are minimized. Parameters are shown in TABLE I. simulations for a 6-cells CHB inverter and

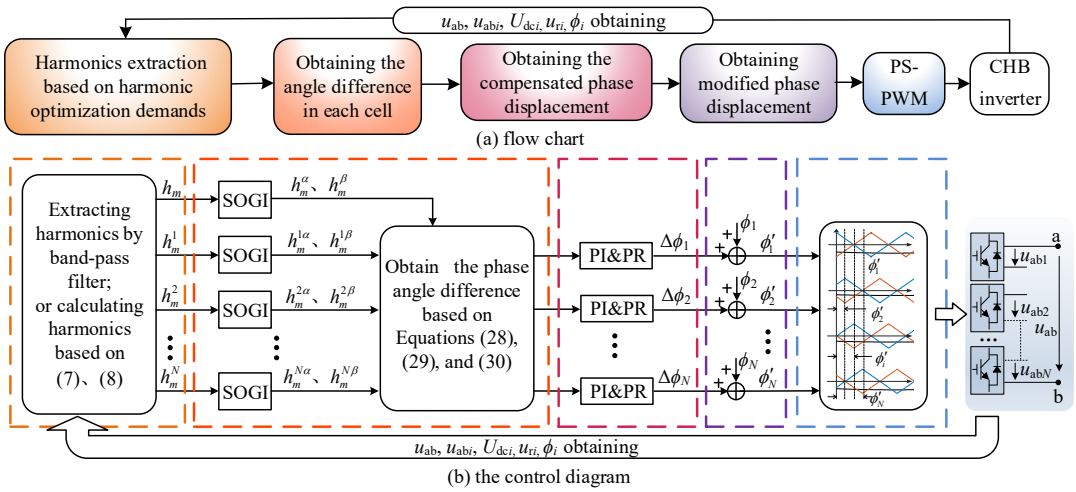

Fig. 10 The control diagram of the proposed closed-loop harmonic suppression scheme.

scaled-down experimental tests for a 4-cells CHB inverter are performed.

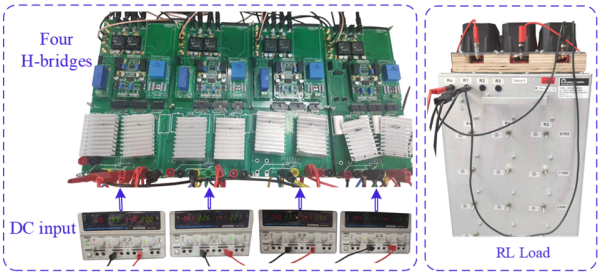

Fig. 11 The experiment platform.

TABLE I
SYSTEM PARAMETERS

Parameters	Value
Switching frequency f_c/Hz	500
The inductance of AC side L_s/mH	6
The resistance load of AC side R_s/Ω	56
The DC-link capacitor C/mF	3.3

TABLE III lists the dc voltages and modulation indices for the 6-cells CHB inverter. Harmonic spectrums comparison with the conventional PS-PWM (Con. PS-PWM) and the proposed method are shown in Fig. 12. Sideband harmonics h_1 (m=1) around the center frequency 1kHz ($2f_c$) and sideband harmonic $h_{1(-1)}$ (m=1, n=-1) at 950Hz, which has the largest amplitude around $2f_c$, are selected to be suppressed. The proposed method evidently shows a good harmonic suppression performance.

TABLE II
SCENARIOS OF UNBALANCED CONDITION

case	DC voltages U_{dci}/V	Modulation indices M_i/p.u.
I	[50 45 53 48 57 43]	[0.83 0.95 0.85 0.97 0.80 0.93]
II	[35 32 30 33 30 110]	[0.98 0.98 0.90 0.97 0.95 0.73]

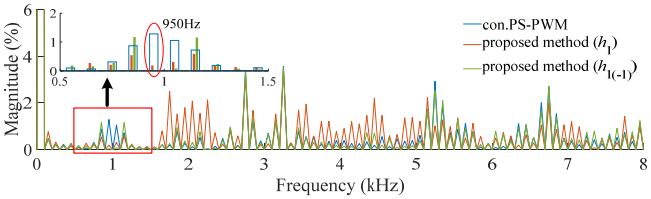

Fig. 12 Suppression of harmonics h_1 and $h_{1(-1)}$ for case I.

Fig. 13 shows the harmonic spectrums comparison of sideband harmonics h_3 and h_{32}, whose vector diagrams are similar to Fig. 9. Obviously, the proposed method is effective to suppress the harmonics h_3 and h_{32}. It verifies the effectiveness of the proposed method to suppress the selected harmonics.

The higher harmonics around 2kHz ($2f_c$), 3kHz ($6f_c$), 4kHz ($8f_c$), and 5kHz ($10f_c$) are increased a bit when the harmonics h_1 and $h_{1(-1)}$ are minimized in Fig. 12. But they do not have a negative impact on the output voltages, since the higher harmonics are easily mitigated by the filter inductor. However, from Fig. 13, although harmonics h_3 and h_{32} are minimized by the proposed method, the lower sideband harmonics around 1kHz ($2f_c$) increase. This drawback results in application limits when the proposed harmonic suppression method is used to minimize higher harmonics. Only when the higher harmonics are necessary to be eliminated and the lower harmonics have no great negative impact on the systems or can be filtered out, the proposed method can be adopted to suppress the selected higher sideband harmonics.

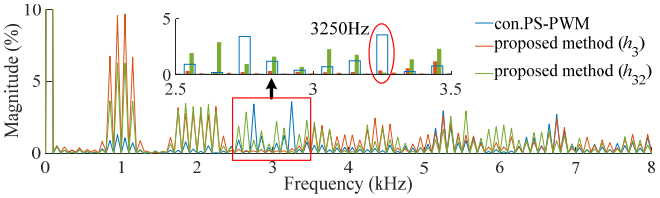

Fig. 13 Suppression of harmonics h_3 and h_{32} for case I.

To verify the effectiveness of the proposed harmonic suppression method for conditions when no closed polygons satisfy the harmonic vectors, the relatively unfavorable operating condition in case II is a good case in point. The magnitudes of sideband harmonics h^i_{10} (1050Hz, m=1, n=0) in each cell can be calculated by (3). Similar to Fig. 8, the harmonic vectors form no closed polygons. But the proposed method can also effectively minimize the sideband harmonics h_1 and h_{10}, as shown in Fig. 14.

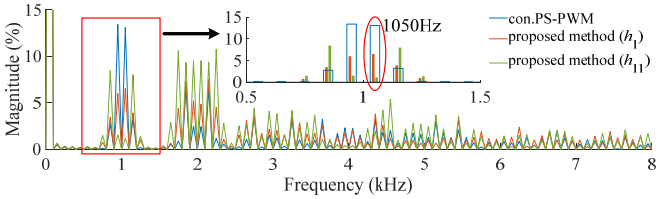

Fig. 14 Suppression of harmonics h_1 and h_{10} for case II.

Experimental tests on 4-cells CHB inverter are additionally conducted to verify the proposed harmonic suppression method. TABLE III lists the three cases: different dc voltages (Case III), different modulation indices (Case IV), dc voltages and modulation indices both different (Case V).

TABLE III
SCENARIOS OF UNBALANCED CONDITION

case	DC voltages U_{dci}/V	Modulation indices M_i/p.u.
III	[40 35 58 50]	[0.95 0.95 0.95 0.95]
IV	[45 45 45 45]	[0.85 0.93 0.89 0.78]
V	[40 60 35 50]	[0.90 0.85 0.95 0.80]

Fig. 15 ~ Fig. 16 describe the harmonic spectrums of the output voltages and the envelope of the harmonics to be suppressed. Considering different dc voltages (Case III) and different modulation indices (Case IV), sideband harmonics around 1kHz ($2f_c$) are selected to be mitigated, since they are the dominant harmonics shown in Fig. 15(a) and Fig. 16(a). Comparing the harmonic spectrums with the Con. PS-PWM and the proposed method, the proposed method is visibly effective to suppress the selected harmonics in Fig. 15(b) and Fig. 16(b). From Fig. 15(c) and Fig. 16(c), the sideband harmonic at 950Hz, which is selected to be mitigated in Case III, can also be suppressed, and the sideband harmonic at 1050Hz in Case IV does likewise. The sideband harmonics envelop H_1 and the sideband harmonic $h_{1(-1)}$, h_{10} in Fig. 15(d) and Fig. 16(d) illustrate the effectiveness of the proposed method more clearly.

Furthermore, Fig. 17 and Fig. 18 describe the harmonic spectrums considering dc voltages and modulation indices both different (Case V). The lower harmonics around 1kHz ($2f_c$) and the selected sideband harmonic at 850Hz are evidently

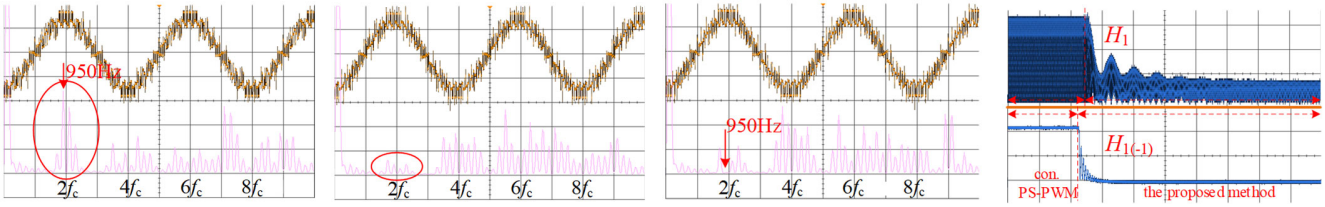

(a) (b) (c) (d)

Fig. 15 Harmonic spectrums and harmonic envelop comparison for Case III. (a) Con.PS-PWM. (b) Harmonic suppression around 1kHz (h_1). (c) Harmonic suppression at 950Hz ($h_{1(-1)}$). (d) Harmonic envelops.

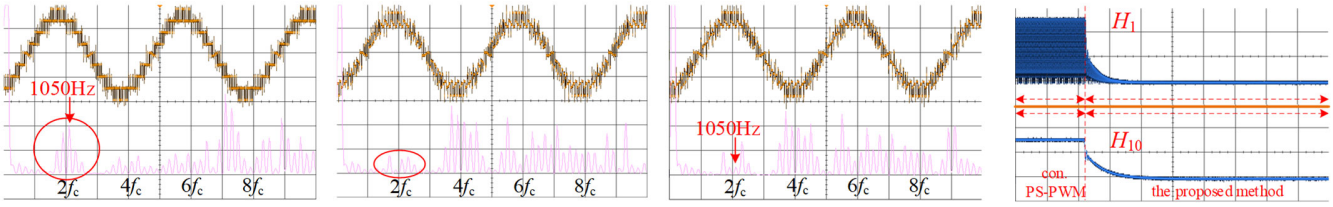

(a) (b) (c) (d)

Fig. 16 Harmonic spectrums and harmonic envelop comparison for Case IV. (a) Con.PS-PWM. (b) Harmonic suppression around 1kHz (h_1). (c) Harmonic suppression at 1050Hz (h_{10}). (d) Harmonic envelops.

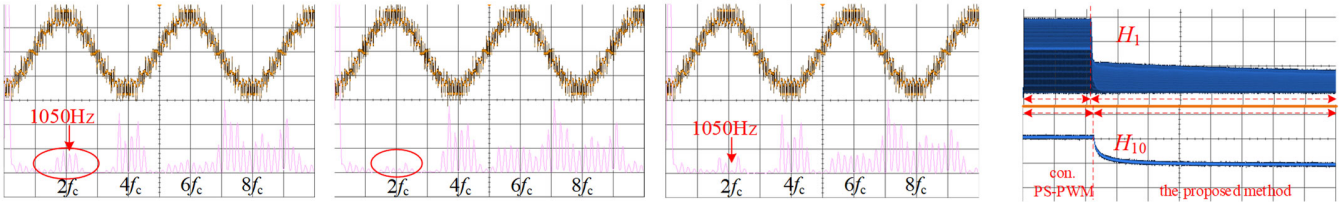

(a) (b) (c) (d)

Fig. 17 Harmonic spectrums and harmonic envelop comparison for Case V. (a) Con.PS-PWM. (b) Harmonic suppression around 1kHz (h_1). (c) Harmonic suppression at 1050Hz (h_{10}). (d) Harmonic envelops.

minimized by the proposed method. Moreover, sideband harmonics around 2kHz ($4f_c$) are also the dominant harmonics. And the vector diagrams of these harmonics are similar to Fig. 9. Fig. 18 illustrates clearly that the proposed method is effective to minimize the sideband harmonics around 2kHz ($4f_c$). Hence, the proposed harmonic suppression method is suitable for the suppression of sideband harmonics summation and one specific sideband harmonic around any multiplicative switching frequency.

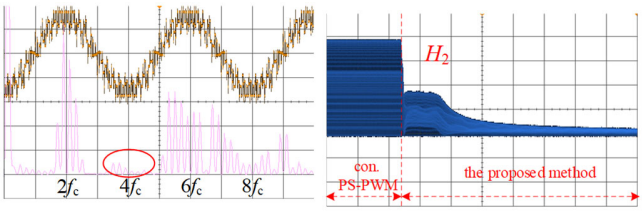

(a) (b)

Fig. 18 Harmonic spectrums and harmonic envelop around $4f_c$ for Case V. (a) Harmonic suppression around $4f_c$ (h_2). (b) Harmonic envelops.

Fig. 19 shows the displacement angles based on the proposed method for the three cases in real-time. The displacement angles achieve continuous adjustment. The displacement angles are evidently regulated to the steady-state by the proposed harmonic suppression method.

V. Conclusions

From the theoretical analysis and the experimental verification in this article, the following conclusions can be drawn:

1) In unbalanced conditions, the harmonic distortion around the selected multiplicative switching frequency can be suppressed by the proposed closed-loop harmonic suppression method in real-time. The one specific sideband harmonic also can be suppressed effectively.

2) The proposed harmonic suppression method for CHB inverters is not limited by cell number.

3) The proposed method is suitable for conditions when the harmonic vectors do not satisfy a closed polygon.

4) Benefiting from the continuous adjustment of the displacement angles, the proposed method is effective for complex operations.

References

[1] W. Mcmurray, “Fast response stepped-wave switching power converter circuit,” U.S. Patent 3 581 212, May 25, 1971. [Online]. Available: https://www.google.com/patents/US3581212

[2] Z. Yang, J. Sun, X. Zha, and Y. Tang, “Power decoupling control for capacitance reduction in cascaded-H-bridge-inverter-based regenerative motor drive systems,” *IEEE Trans. Power Electron*., vol. 34, no. 1, pp. 538–549, Jan. 2019.

[3] J. I. Leon, S. Kouro, L. G. Franquelo, J. Rodriguez, and B. Wu, “The essential role and the continuous evolution of modulation techniques for voltage-source inverters in the past, present, and future power electronics,” *IEEE Trans. Ind. Electron.*, vol. 63, no. 5, pp. 2688–2701, May 2016.

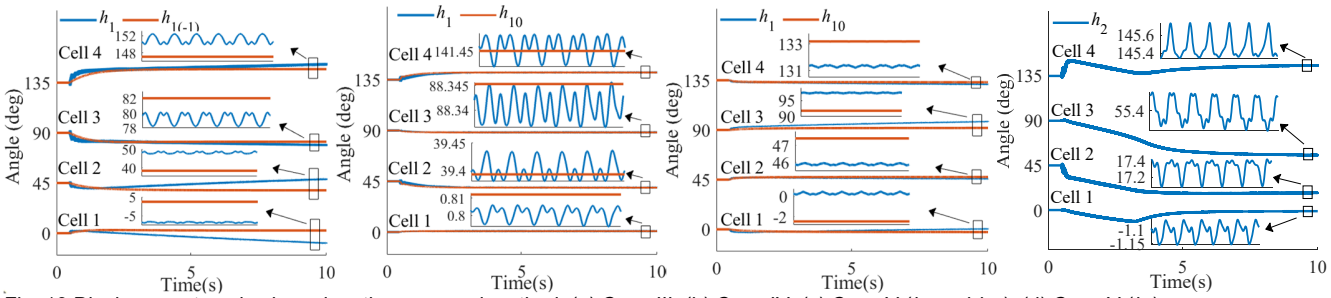

Fig. 19 Displacement angles based on the proposed method. (a) Case III. (b) Case IV. (c) Case V (h_1 and h_{10}). (d) Case V (h_2).

[4] C. Liu, F. Deng, Q. Yu, Y. Wang, F. Blaabjerg, and X. Cai, "Submodule Capacitance Monitoring Strategy for Phase-Shifted Carrier Pulsewidth Modulation-Based Modular Multilevel Converters," *IEEE Trans. on Ind. Electron*., vol. 68, no. 9, pp. 8753 - 8767, 2020.

[5] V. G. Monopoli, Y. Ko, G. Buticchi and M. Liserre, "Performance Comparison of Variable-Angle Phase-Shifting Carrier PWM Techniques," *IEEE Trans. Ind. Electron.*, vol. 65, no. 7, pp. 5272-5281, July 2018.

[6] N. Jiao, S. Wang and T. Liu, "Analysis of Load Balancing Limits for Cascaded Rectifiers," *2018 IEEE 4th Southern Power Electronics Conference (SPEC)*, 2018, pp. 1-7.

[7] S. Wang, N. Jiao, J. Ma, T. Liu and X. Liu, "Analysis and Optimization of Voltage Balancing Control Limits for Cascaded H-Bridge Rectifiers," *IEEE Trans. Ind. Electron.*, vol. 68, no. 11, pp. 10677-10687, Nov. 2021.

[8] L. Liu, H. Li, Z. Wu, and Y. Zhou. "A Cascaded Photovoltaic System Integrating Segmented Energy Storages With Self-Regulating Power Allocation Control and Wide Range Reactive Power Compensation," *IEEE Trans. Power Electron*, 2011, 26(12): 3545-3559.

[9] V. G. Monopoli, A. Marquez, J. I. Leon, Y. Ko, G. Buticchi, and M. Liserre, "Improved harmonic performance of cascaded H-bridge inverters with thermal control," *IEEE Trans. Ind. Electron.*, vol. 66, no. 7, pp. 4982–4991, Jul. 2019.

[10] Y. Li, Y. Wang and B. Q. Li, "Generalized Theory of Phase-Shifted Carrier PWM for Cascaded H-Bridge Converters and Modular Multilevel Converters," *IEEE J. Emerg. Sel. Topics Power Electron*., vol. 4, no. 2, pp. 589-605, June 2016.

[11] A. Marquez, J. I. Leon, V. G. Monopoli, S. Vazquez, M. Liserre, and L. G. Franquelo, "Generalized Harmonic Control for CHB Inverters With Unbalanced Cells Operation," *IEEE Trans. Ind. Electron*., vol. 67, no. 11, pp. 9039-9047, Nov. 2020.

[12] A. Marquez, "High-quality output voltage of multilevel cascaded h-bridge inverters with large number of cells with unequal DC voltages," in *Proc. IEEE 13th Int. Conf. Compat. Power Electron. Power Eng.*, Apr. 2019.

[13] V. G. Monopoli et al., "Applications and Modulation Methods for Modular Converters Enabling Unequal Cell Power Sharing: Carrier Variable-Angle Phase-displacement Modulation Methods," *IEEE Ind. Electron.s Mag*., doi: 10.1109/MIE.2021.3080232.

[14] A. Marquez, J. I. Leon, R. Portillo, S. Vazquez, L. G. Franquelo and S. Kouro, "Adaptive phase-shifted PWM for multilevel cascaded H-bridge converters for balanced or unbalanced operation," *IECON 2015 - 41st Annual Conference of the IEEE Ind. Electron. Soc.*, 2015, pp. 005124-005129

[15] A. Marquez et al., "Variable-Angle Phase-Shifted PWM for Multilevel Three-Cell Cascaded H-Bridge Converters," *IEEE Trans. on Ind. Electron*., vol. 64, no. 5, pp. 3619-3628, May 2017.

[16] A. Marquez, J. I. Leon, S. Vazquez, L. G. Franquelo and S. Kouro, "Operation of an hybrid PV-battery system with improved harmonic performance," *IECON 2017 - 43rd Annual Conference of the IEEE Ind. Electron. Soc.*, 2017, pp. 4272-4277.

[17] F. Eroglu, A. O. Arslan, M. Kurtoglu, and A. M. Vural, "Generalized adaptive phase-shifted PWM for single-phase seven-level cascaded H-bridge multilevel inverters," *2018 5th International Conference on Electrical and Electronic Engineering (ICEEE)*, 2018, pp. 7-12.

[18] A. Marquez et al., "Sampling-Time Harmonic Control for Cascaded H-Bridge Converters With Thermal Control," *IEEE Trans. on Ind. Electron*., vol. 67, no. 4, pp. 2776-2785, April 2020.

[19] A. Marquez, J. I. Leon, S. Vazquez, L. G. Franquelo and S. Kouro, "Adaptive phase-shifted PWM for multilevel cascaded H-bridge converters with large number of power cells," *2017 11th IEEE International Conference on Compatibility, Power Electronics and Power Engineering (CPE-POWERENG)*, 2017, pp. 430-435.

[20] A. M. Alcaide et al., "Variable-Angle PS-PWM Technique for Multilevel Cascaded H-Bridge Converters With Large Number of Power Cells," *IEEE Trans. on Ind. Electron*., vol. 68, no. 8, pp. 6773-6783, Aug. 2021.

[21] A. Marquez et al., "Discontinuous-PWM Method for Multilevel N-Cell Cascaded H-Bridge Converters," *IEEE Trans. on Ind. Electron*., vol. 68, no. 9, pp. 7996-8005, Sept. 2021.

[22] P. Liu and S. Duan, "Derivation of the Generalized Phase-Shifted Angles by Using Phasor Diagrams for the CHB Converter With Unbalanced DC Voltage Sources," *IEEE Trans. on Ind. Electron*., vol. 68, no. 12, pp. 12002-12009, Dec. 2021.

[23] D. Holmes and T. Lipo, Pulse Width Modulation for Power Inverters: Principles and Practice. Hoboken, NJ, USA: Wiley, 2003.